Acta Materialia 220 (2021) 117298

Contents lists available at ScienceDirect

Acta Materialia

journal homepage: www.elsevier.com/locate/actamat

Full Length Article

Positron annihilation investigation of thermal cycling induced martensitic transformation in NiTi shape memory alloy

M. Liu[a,1], P. Diercks[a], A. Manzoni[a,b], J. Čížek[c], U. Ramamurty[d,e], J. Banhart[a,*]

[a] Helmholtz-Zentrum Berlin, Hahn-Meitner-Platz 1, Berlin 14109, Germany
[b] Bundesanstalt für Materialforschung und -prüfung, Unter den Eichen 87, Berlin 12205, Germany
[c] Charles University, V Holešovičkách 2, Praha 8 18000, Czech Republic
[d] School of Mechanical and Aerospace Engineering, Nanyang Technological University, Singapore 639798, Republic of Singapore
[e] Institute of Materials Research Engineering, Agency for Science, Technology and Research, Singapore 138634, Republic of Singapore

ARTICLE INFO

Article history:
Received 28 June 2021
Revised 16 August 2021
Accepted 3 September 2021
Available online 8 September 2021

Keywords:
Shape memory alloy
Thermal cycling
Defects
Positron annihilation spectroscopy
Austenite-to-martensite phase transformation

ABSTRACT

Thermal cycling of a Ni-excess NiTi alloy was conducted between 50 °C and liquid nitrogen temperature to induce martensitic transformations and to reverse them after. The starting point was an annealed and slowly cooled state, the end point a sample thermally cycled 1500 times. Positron annihilation lifetime spectra and Coincidence Doppler Broadening profiles were obtained in various states and at various temperatures. It was found that the initial state was low in defects with positron lifetimes close to that of bulk NiTi. Cycling lead to a continuous build-up of a defect structure up to 200–500 cycles after which saturation was reached. Two types of defects created during cycling were identified, namely pure dislocations and vacancies attached to dislocations.

1. Introduction

Near-equiatomic NiTi shape memory alloys (SMAs) exhibit pseudoelasticity and the shape-memory effect and like many other SMAs have promising application prospects. Their physical metallurgy is complicated and processes on the micro and mesoscale vary with alloy composition and thermomecanical pre-treatment. A one-step martensitic transformation B2 → B19' is observed in near equiatomic alloys with a slight Ni excess that are quenched from the homogenisation temperature [1]. The exact Ni content–usually between 50 and 51 at.% – has a pronounced influence on transformation temperature. Two-step transformation via the *R* phase occurs in annealed alloys [2].

Training of SMAs by thermal cycling can increase fatigue life in NiTi(Fe) alloys [3] and it is such thermal cycling that will be studied in this paper. Thermal cycling induces dislocation substructures that are not uniformly distributed due to their mutual interactions. Cycling can hinder transformation [4,5], i.e. shift the associated DSC peak to lower temperatures, or have the opposite effect [6,7].

Positron annihilation spectroscopy (PAS) is a powerful materials characterization tool for investigating atomic level changes caused by point or line defects. It relies on the annihilation of positrons with electrons in a sample. Lifetime spectroscopy exploits the lifetime differences between areas of higher electron densities (short lifetimes in defect-free areas of the alloy) and lower electron density (longer lifetimes in vacancies, dislocations, other open volume) and thus allows one to identify structural features. Coincidence Doppler broadening (CDB) spectroscopy makes use of the annihilation signature of a positron with the core electrons of the atoms surrounding an annihilation site (e.g. a vacancy) and provides chemical information. Due to PAS's high sensitivity, it is expected that minute structural changes that occur during thermal cycling of SMAs can be detected.

The few applications of PAS to NiTi alloys published so far have revealed only a few basic properties such as the positron lifetime in a defect-free NiTi bulk (measurements on melt-spun and annealed alloys [8]), the lifetime in vacancies induced by electron irradiation [9] or positron lifetime changes in the pre-martensitic region or at the onset of martensitic transformation [10–12]. The results are not always consistent. It has been reported that thermal cycling of melt-spun NiTi alloys has little effect on positron lifetime due to the high defect density in such materials. This is why we decided to cycle materials with a low defect density to be able to isolate the effect of cycling. Often, NiTi alloys are quenched

* Corresponding author.
E-mail address: banhart@helmholtz-berlin.de (J. Banhart).
[1] Present address: Chinalco Materials Application Research Institute, Future Science, Changping District, Beijing, PR China.

https://doi.org/10.1016/j.actamat.2021.117298

from a high homogenisation temperature (e.g. 1000 °C) prior to further characterization. Such quenching induces defects in many alloys and, for example, in aluminium alloys the positron lifetime after quenching is very different from that of an annealed material and also changes with time at 'room temperature' [13]. In NiTi alloys, however, the mean positron lifetime after quenching is not much higher than after annealing [10] (0.138 ns compared to 0.130 ns) and much lower than in irradiated alloys (0.197 ns [9]) and therefore not many quenched-in vacancies seem to exist. As quenching stresses might give rise to the formation of dislocations, we used an annealed and slowly cooled state for our studies. The possible formation of Ti_3Ni_4 precipitates and associated *R* phase formation during subsequent cooling to low temperature [14] was deemed relatively less of a concern than the formation of defects that would obscure the signal from defects induced by thermal cycling.

An alloy prepared in this way was investigated by PAS at 20 °C during cycling and also at lower temperatures for selected states to detect open atomic volume created by cycling and to reveal the nature of the associated defects.

2. Experimental

NiTi alloy was provided by Special Metals Corp., USA, and is the same used in a previous study [15] and characterized there as room temperature austenite. In the solutionized and quenched state it exhibits a one-step transformation from austenite to martensite with the following transformation temperatures: Martensite start, M_s = 2.1 °C, Martensite finish, M_f = −41.4 °C, Austenite start, A_s = −1.3 °C, Austenite finish, A_f = 23 °C [15]. From published relationships between Ni content and transformation temperature M_s for binary alloys we derive an effective Ni content of 50.55 ± 0.05 at.% [16]. The samples were received as rolled sheets of 0.6 mm thickness.

The as-received condition is abbreviated 'AR' here after. The starting material was annealed at 800 °C for 30 min in an argon atmosphere containing 0.1 ppm residual oxygen and then slowly cooled to 'room temperature' in 1 day. This state will be abbreviated 'AN' in the following. One sample was quenched in ice water (referred as 'AQ'). The AN samples were thermally cycled between 50 and −196 °C up to 1500 times using an in-house fabricated robotic system that dipped the sample into liquid nitrogen, after which it was pulled out and heated to 50 ± 3 °C using a hot air blower. Samples cycled *n* times will be called 'C*n*' in the following. C1 means that the AN sample was cooled to −196 °C, reheated to 50 °C and then characterized at 20 or 25 °C ('room temperature') by positron annihilation spectroscopy (PAS) or transmission electron microscopy (TEM). Some samples were cycled by cooling down to −125 °C in a cryostat while carrying out PAS measurements at various temperatures and then reheating again. One sample was left at 'room temperature' for 2 months during which positron lifetime was measured.

Two positron lifetime spectrometers were used. The one at the laboratory in Berlin (*B*) is an analogue fast–fast coincidence spectrometer with photomultiplier tubes H3378–50 from Hamamatsu and BaF_2 scintillators. Backscattering was suppressed by lead shields [17]. The count rate achieved was 700–800 s^{-1}. The measured positron lifetime spectra with typically 2 × 10^6 counts contain contributions from the 20 µCi $^{22}Na_2CO_3$ source itself. We used spectra measured on pure annealed Ni and Ti to determine the contributions of the positron source to the measured spectra. They contain a component of about 15% from the two 7.5 µm thick Kapton foils and the sodium salt (∼0.380 to ∼0.400 ns) and less than 1% of a component with a long (∼3 ns) lifetime due to surfaces and pores and other contributions. For this component, we adopted the strategy outlined in Ref. [13] to treat the lifetime and intensity of that component as a variable and to check whether it takes reasonable values after fitting. Computer programme LT9 was used to subtract the source contributions as well as the background and to de-convolute the spectra from the spectrometer resolution function [18], which we found to be well represented by one Gaussian with a FWHM of ∼0.220 ns.

The spectrometer in Prague (*P*) is digital and optimised for high resolution (FWHM of resolution function is 0.145 ns) but has a much lower count rate of 50 s^{-1} [19]. The spectrometer is equipped with BaF_2 scintillators optically coupled to Hamamatsu H3378–50 photomultiplier tubes. Pulses from the detectors are sampled by a pair of Acqiris DC211 digitisers at a rate of 4 GHz. The 27 µCi ^{22}NaCl positron source is sealed by a 2 µm thick titanium foil. Decomposition of positron lifetime spectra is analogous to the treatment in Berlin except that the spectrometer resolution function is modeled by two Gaussians [19]. The source contribution to the positron lifetime spectra was determined using a reference sample of well-annealed iron and its intensity was recalculated for the NiTi SMA specimens using the procedure described in Ref. [20]. The source contribution consisted of two components with lifetimes ∼0.180 and ∼0.400 ns and relative intensities ∼11% and ∼2%, respectively. These components represent a contribution of positrons annihilated in the Ti foil and the ^{22}NaCl positron source spot, respectively. The corrections were measured at 20 °C and at −125 °C and found to be almost the same. 5 × 10^6 counts were obtained for each spectrum which took typically a day. All the measurements were carried out in a cryostat that guaranteed a temperature stability of ± 5 K. Analysis of the positron spectra yielded a one-component positron lifetime τ_{1C} whenever just one positron lifetime was suspected. Alternatively, two lifetime components were derived, and 3 corresponding independent parameters obtained, namely two lifetimes and one intensity.

The CDB investigations were carried out using a digital spectrometer [21] equipped with two HPGe detectors. The detector signals are sampled by 12-bit digitizers Acqiris DC 440 and analysed off-line using a dedicated computer code [21]. The spectrometer is characterized by an energy resolution of 0.9 at 511 keV and a peak-to-background ratio better than 10^5. At least 5 × 10^6 annihilation events were accumulated in each two-dimensional CDB spectrum which was subsequently reduced to one-dimensional cuts representing the resolution function of the spectrometer and the Doppler-broadened annihilation photo peak. In order to highlight the high-momentum region, the CDB results are presented as ratio curves [22] related to an aluminium reference, i.e. a normalised momentum distribution of each sample was divided by the normalised momentum distribution of a well-annealed pure Al (99.9999%) reference sample. Similar to positron lifetime studies, the CDB measurements were also carried out in a cryostat with temperature stability of ± 5 °C.

Thermal analysis was performed on 4.8 mm diameter disc samples using a Netzsch 204 F1 Phoenix differential scanning calorimeter at a heating rate of 10 K/min. A baseline obtained by heating two empty crucibles at the same heating rate was subtracted.

Samples for TEM were prepared by electropolishing at a temperature of −30 °C and a voltage of 20 V using an electrolyte consisting of 59% methanol, 35% diethylene glycol butyl ether and 6% perchloric acid (by volume). Two TEMs were used in this study: A TEM Philips CM30 (ThermoFischer Scientific) operated at 300 kV and at 'room temperature' and a JEOL 2200 FS operated at 200 kV and at liquid nitrogen temperature.

3. *Ab-inito* calculations

Ab-initio calculations were employed for modeling vacancies in the cubic B2 NiTi structure [23], the trigonal (rhombohedral) *R*

Table 1
Lifetime τ calculations of positrons delocalized in a perfect lattice (bulk lifetime) or trapped in Ni (V_{Ni}) or Ti (V_{Ti}) vacancies based on given lattice parameters. Calculated positron binding energies E_B to vacancies are also listed. The mean displacements of the nearest neighbour (NN) and next nearest neighbour (NNN) ions surrounding vacancies obtained from *ab-initio* calculations are shown in the last two columns. Negative values indicates inward relaxation (towards vacancy), positive values indicate outward relaxation in the direction out of the vacancy.

Phase	Space group	Lattice parameters	Positron state	τ (ns)	E_B (eV)	NN relaxation (Å)	NNN relaxation (Å)
B2	$Pm\bar{3}m$	$a = b = c\sqrt{2}$ c= 3.013 Å [23]	bulk	0.127	–	–	–
			V_{Ni}	0.194	2.69	−0.12 (Ti)	0.10 (Ni)
			V_{Ti}	0.207	5.96	0.12 (Ni)	−0.05 (Ti)
R	$P\bar{3}$		bulk	0.131	–	–	–
		$a = b$ = 7.3451 Å c = 5.2718 Å γ = 120 ° [25]					
			V_{Ni}	0.199	2.86	−0.09 (Ni)	0.09 (Ni)
			V_{Ti}	0.207	3.87	0.10 (Ti)	−0.10 (Ti)
B19'	$P2_1/m$	a = 4.66 Å b = 4.11 Å c = 2.91 Å γ = 98 ° [24]	bulk	0.129	–	–	–
			V_{Ni}	0.195	4.66	−0.14 (Ni)	0.12 (Ni)
			V_{Ti}	0.207	5.90	0.15 (Ti)	−0.16 (Ti)

phase [24] and the monoclinic B19' phase [25]. The lattice parameters of these phases are listed in Table 1. Vacancies in the B2 and B19' phases were modeled using 108-atom based supercells, while 144-atom supercells were used for the *R* phase. Electronic structure calculations and ion relaxation around vacancies were performed using the projector augmented wave (PAW) method [26] implemented in the Vienna *Ab-initio* Simulation Package (VASP) [27,28]. An electron exchange-correlation potential of Perdew–Burke–Ernzerhof (PBE) [29] was used. The energy cut-off of the plane wave basis of 500 eV and Fermi smearing of the electronic occupancy with a width of 0.2 eV were used in all calculations. Reciprocal space was sampled using a 3 × 3 × 3 *k*-point mesh generated applying the Monkhorst-Pack scheme [30]. Convergence tests revealed that calculated energies converged to within ≈0.01 eV. Equilibrium geometries of defects were determined by fully relaxing ions positions in the supercell as well as supercell volume. Structural relaxations were performed until forces on each atom were smaller than 0.01 eV/Å.

Lifetimes of free positrons and positrons trapped in vacancies were calculated using density functional theory. The ground state densities for both positrons delocalized in a perfect lattice and trapped at various defects were calculated within the so-called conventional scheme [31]. In this approximation, the positron density is vanishingly small everywhere and does not affect the bulk electron structure. At first, the electron density $n(\boldsymbol{r})$ in the material is solved without the positron. Subsequently, the effective potential for a positron is constructed as:

$$V_+(\boldsymbol{r}) = \varphi(\boldsymbol{r}) + V_{\text{corr}}[n, \nabla n], \tag{1}$$

where $\varphi(\boldsymbol{r})$ is the Coulomb potential produced by the charge distribution of electrons and nuclei and V_{corr} is the zero positron density limit of the electron-positron correlation potential [31]. The ground state positron wave function was calculated by a numerical solution of a single-particle Schrödinger equation:

$$-\frac{1}{2}\nabla^2\psi_+(\boldsymbol{r}) + V_+(\boldsymbol{r})\psi_+(\boldsymbol{r}) = E_+\psi_+(\boldsymbol{r}), \tag{2}$$

where E_+ is the positron ground state energy. The positron lifetime was calculated from the overlap of the positron density $n_+(\boldsymbol{r}) = |\psi_+(\boldsymbol{r})|^2$ and the electron density $n(\boldsymbol{r})$ using the expression:

$$\tau = \left\{\pi r_e^2 c \int n_+(\boldsymbol{r}) n(\boldsymbol{r}) \gamma[n, \nabla n] d\boldsymbol{r}\right\}^{-1}, \tag{3}$$

where r_e is the classical electron radius, and c is the speed of light. The electron enhancement factor γ accounts for the pile-up of electrons at the positron site [31]. The electron-positron correlation potential and the enhancement factor were treated by the generalized gradient approximation (GGA) using the approach where V_{corr} and γ are determined by the electron density n and its gradient ∇n at the site of positron [32]. A Brillouin-zone integration over the lowest-lying positron state [33] was used in calculations of positron density for vacancies to achieve rapid convergence of the results with respect to the supercell size. Positron calculations were performed using relaxed geometries of defects obtained from VASP. For calculations of positron density, the supercells used in VASP were enveloped by a perfect lattice of the corresponding phase in order to get larger supercells, namely a 256-atom based supercell for the B2 and B19' phase and a 1152-atom based supercell for the *R* phase. The electron density $n(\boldsymbol{r})$ for positron calculations in Eqs. (1)–(3) was constructed by superposition of atomic electronic densities calculated using a relativistic atomic code [34]. This approach called *atomic superposition* [35] neglects charge transfer, but it is computationally feasible and can be used even for very large supercells retaining the full 3D geometry of the problem.

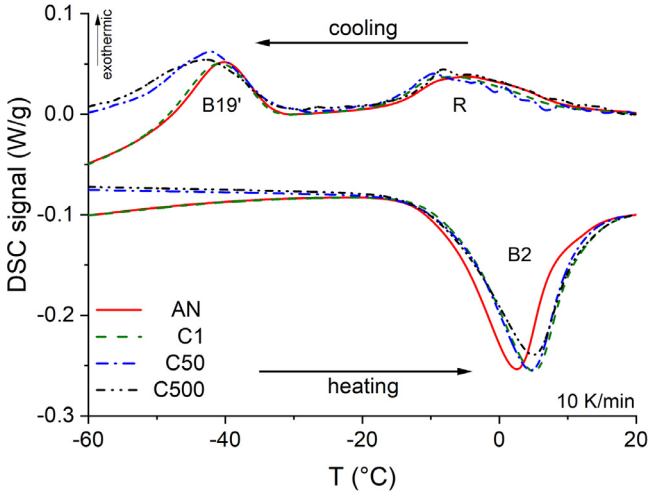

Fig. 1. DSC measurements on NiTi alloy in state AN and after various thermal cycles (Cn). The zero point of all curves is at 20 °C. The lower curves are offset by −0.1 W/g to avoid overlap with the upper.

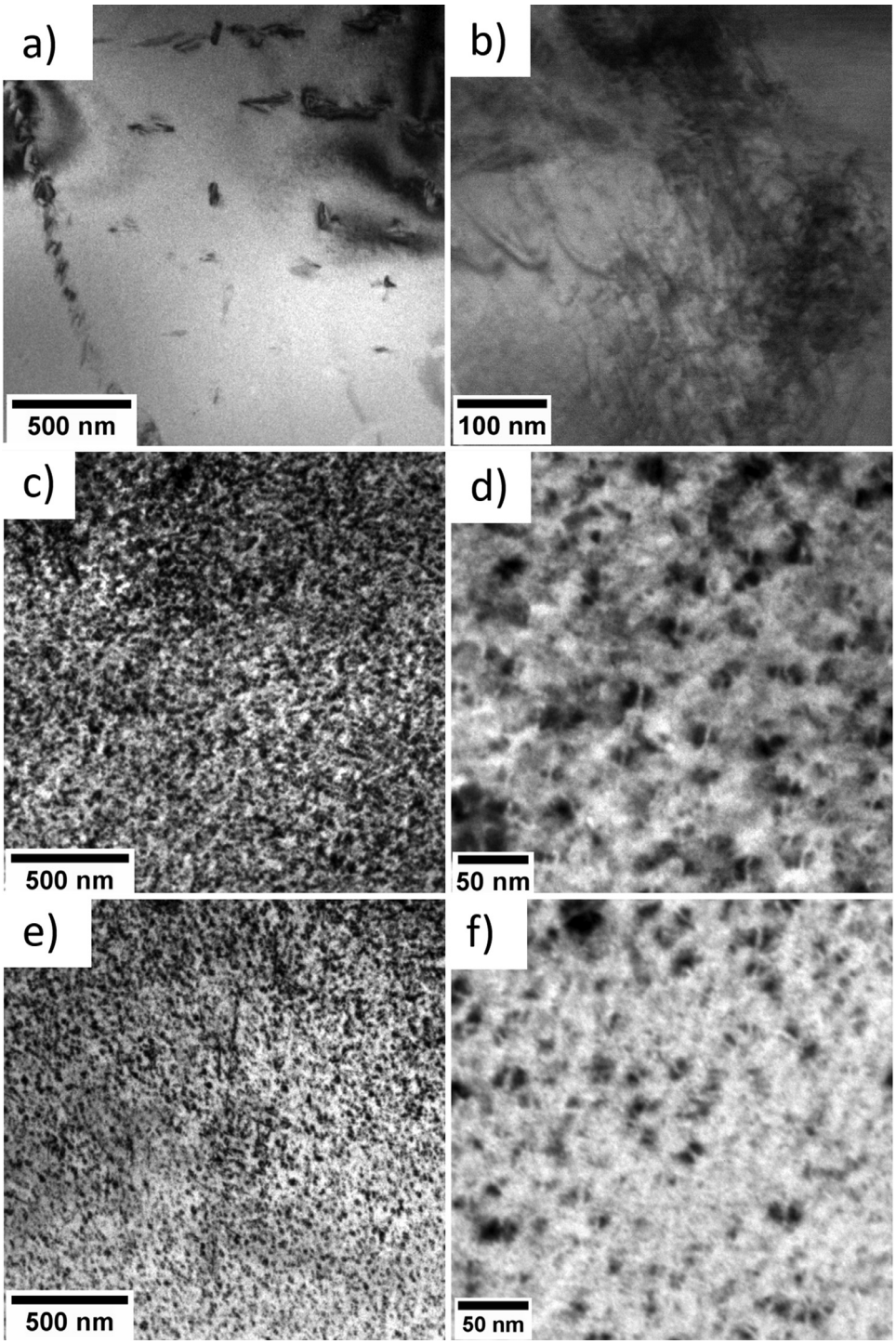

Fig. 2. TEM BF images, taken in the 110 two-beam condition, (a) annealed and slowly cooled (AN), (b) annealed and quenched (AQ), (c, d) sample C1 in 2 magnifications, (e, f) sample C1500 in 2 magnifications.

4. Results

Fig. 1 gives the thermal traces obtained for the annealed NiTi sample (AN) from 60 to −100 °C and back to 60 °C (only central temperature range shown) and for samples thermally cycled 1, 50 and 500 times before DSC measurement. In all cases, two peaks upon cooling and one upon heating are measured. A slight shift to lower or higher temperatures for increasing cycling numbers during cooling or heating, respectively, can be seen.

Fig. 2 shows various microstructures obtained by TEM. The annealed sample ('AN'), Fig. 2a, features little contrast and in particular no pronounced presence of dislocations unlike the quenched sample ('AQ') in which dislocations are visible, Fig. 2b. The sample cycled once ('C1') exhibits a different scenario: it is full of dark contrast, Fig. 2c, which at higher magnification becomes visible as about 10–20 nm large objects, most of which in black with a white division line ('coffee-beans'), see Fig. 2d. TEM images of samples cycled 500 (not shown) and 1500 times, Fig. 2e, f, look similar to

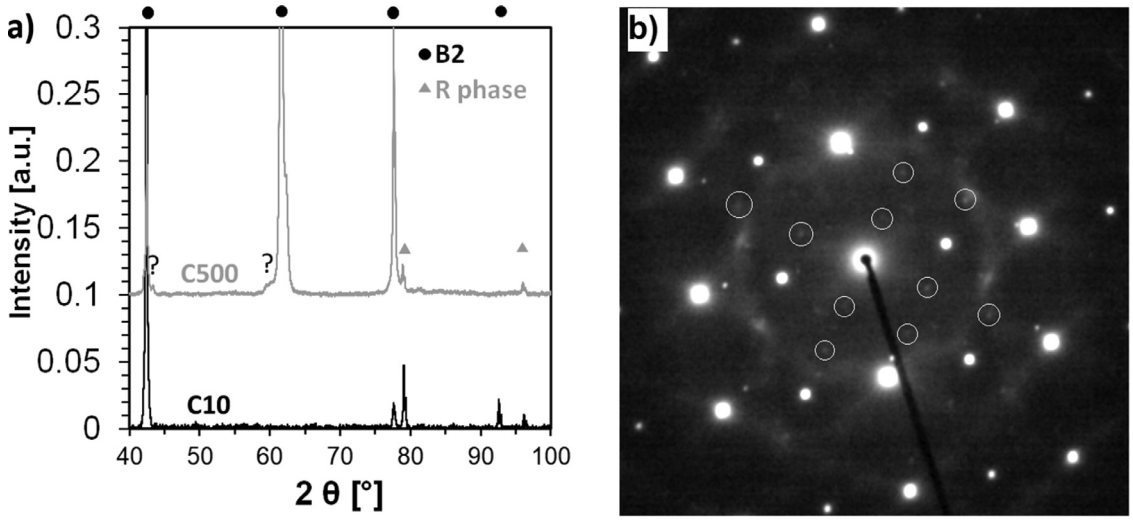

Fig. 3. Diffraction analysis of NiTi samples: (a) XRD pattern recorded on the samples cycled 10 times (C10) and 500 times (C500), showing the B2 and *R* phase peaks. Due to the large grain size (up to 500 μm) only a few grains contribute to the recorded diffracted signal and therefore the intensity ratios between the peaks markedly vary. (b) SAED pattern recorded along the $[110]_{B2}$ axis of the C500 sample showing *R* phase peaks in the circles.

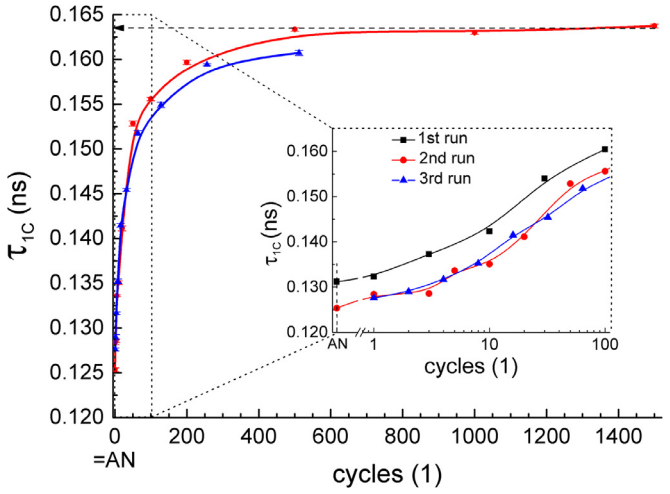

Fig. 4. One-component positron lifetime τ_{1C} for annealed state AN as well as for cycled states Cn measured at 20 °C in spectrometer *B*. Inset shows data for $n \leq 100$ on a logarithmic cycle scale.

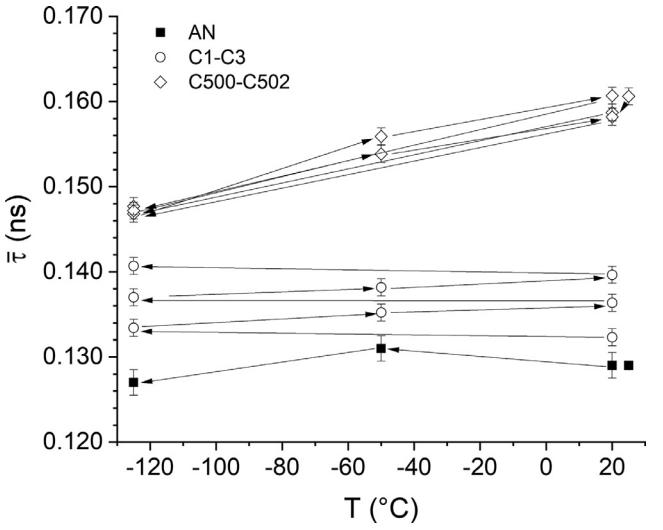

Fig. 5. Averaged lifetime $\bar{\tau}$ measured at 4 temperatures for samples AN, C1 (then C2, C3) and C500 (then C501, C502) using spectrometer *P*. Arrows indicate sequence of cooling or heating.

those of sample C1 with a dense collection of objects with predominantly coffee-bean contrast. It is hard to judge, whether the number density of particles in samples C500 and C1500 is higher than in C1 due to high contrast and uncertain thickness of the area imaged.

The nature of these particles was further studied by means of X-ray and electron diffraction. Fig. 3a shows X-ray diffraction (XRD) patterns of samples C10 and C500 and Fig. 3b the selected area diffraction pattern recorded in the TEM on a C500 sample, taken along the 110 zone axis of the B2 phase. *R* phase spots are highlighted with circles. The diffraction experiments show that the phase formed during thermal cycling of the annealed TiNi alloy has the structure of the *R* phase. The small non-labelled peaks do not correspond to Ni_4Ti_3 phase, i.e., no trace of this phase is detected.

The variation of the one-component positron lifetime τ_{1C} measured at 20 °C with spectrometer *B* as a function of the number of thermal cycles is shown in Fig. 4. The measured lifetime values increase from (0.129-0.131=uncertainty) ns to 0.163 ns for the annealed state up to 0.163 ns for 500 and more thermal cycles. The largest slope is observed for the initial cycles and the increase levels off after about 200–500 cycles (arrow in Fig. 4). The various runs differ only marginally. Especially the first that was carried out a few months before the 2nd and 3rd with another spectrometer calibration (inset in Fig. 4).

The temperature dependence of positron lifetime is displayed in Fig. 5. The data were measured with the spectrometer *P*, decomposed into 2 lifetime values and then averaged to $\bar{\tau}$, which might slightly differ from τ_{1C}. Two separate measurements have been merged: one first measured only at 25 °C, three more carried out at different temperatures, 20, −50, and −125 °C. For sample AN, the temperature dependence is marginal. Upon cooling, $\bar{\tau}$ first increases, then decreases again. Such a behavior (for τ_{1C}) was independently confirmed with spectrometer *B* (not shown). Note that the measurement on AN that involves cooling to a temperature below M_f itself is half a cycle. After cycling an annealed sample to the C1 state, the measurement was performed at decreasing temperatures again. This time $\bar{\tau}$ slightly increases. Upon reheating to 'room temperature' the increase is even larger. After this measurement, the sample that was in C1 state initially has been cy-

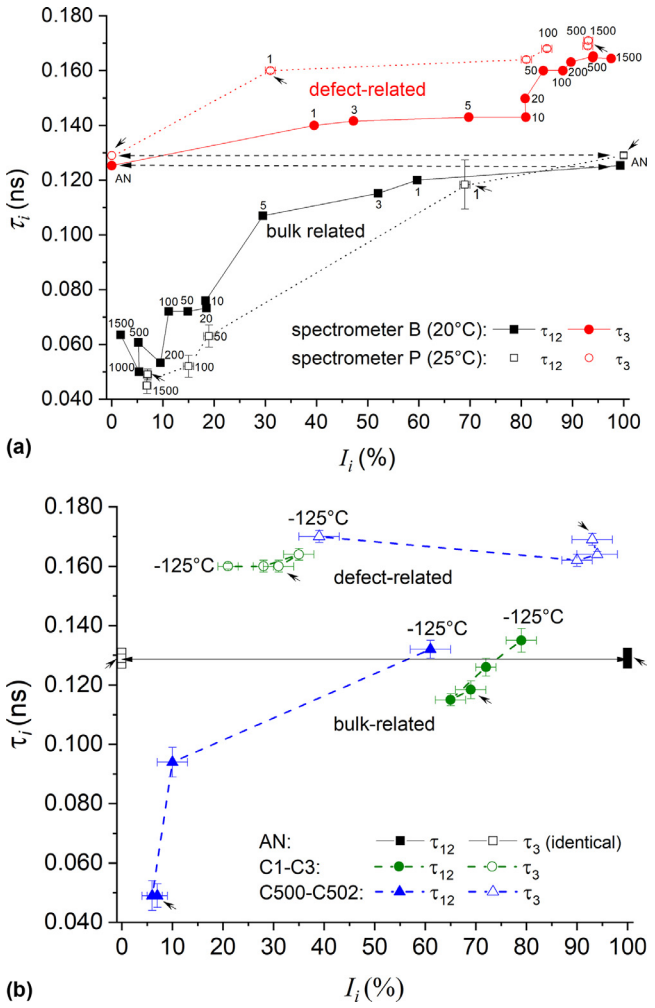

Fig. 6. Two-component decompositions of spectrometer data into τ_{12} and τ_3 for various cycle numbers (0 = AN up to C1500) and temperatures. (a) 'room temperature' measurements for different cycles and spectrometers *B* and *P*. For spectrometer *B*, the error bars have been omitted for the sake of clarity. They are typically ± 0.01 ns for τ and ± 2% for *I*. (b) measurements with spectrometer *P* and the three states AN, C1-C3 (averaged), C500–502 (averaged) at various temperatures. For AN, there is only one component, hence two identical entries connected by an arrow. The low temperature side of each series is marked with '−125 °C'. The small arrows in (a) and (b) point at data points common to both graphs.

cled, hence it is in state C2. The measurement cycle is repeated and leads to an analogous result: $\bar{\tau}$ increases during cooling and heating, slightly more during heating. The resulting sample is then in state C3 and experiences an analogous increase of $\bar{\tau}$ upon further measurement. After 500 cycles the level of $\bar{\tau}$ remains constant between cycle numbers 500 and 502 within the typical experimental fluctuation. An increase of temperature involves a more pronounced increase of $\bar{\tau}$ than for states C1–C3 and a decrease a corresponding larger decrease.

Positron spectra were decomposed into two components, see Fig. 6, where two positron lifetime components τ_{12} and τ_3 are given as a function of their corresponding intensities I_{12} and I_3. Here, the subscript "12″ is chosen because this component will later be found to consist of an average of two components τ_1 and τ_2. Fig. 6a displays 'room temperature' measurements. One set of measurements performed at 20 °C (11 states) was obtained with spectrometer *B*. The corresponding one-component lifetimes were already shown in Fig. 4. The other set was measured with spectrometer *P* at 25 °C (6 cycling states). Two-component decomposition of the lifetime spectra measured at *B* was supported by the results from *P* to set starting conditions of the fitting procedure. Despite some differences between the results of *B* and *P*, the overall trend is the same for both spectrometers: the annealed state can be described by one lifetime component ~0.130 ns but cycling introduces a second component, thus splitting the spectrum into lifetimes τ_{12} and τ_3 with corresponding intensities I_{12} and I_3. Component τ_3 assumes values between 0.160 and 0.169 ns with an increasing intensity contribution I_3 that reaches 93% or more after 1500 cycles. Component τ_{12} decreases from ~0.130 to below ~0.060 ns while I_{12} goes down to a few%.

Fig. 6b shows the lifetime components measured with spectrometer *P* for 3 different cycling states at 4 temperatures. For state AN, there is only one lifetime component and this is only weakly temperature dependent as already seen in Fig. 5. In contrast, data for states C1−C3 and C500−C502, both averaged, are temperature dependent, more for the latter than for the former. Lowering the temperature has the same effect on both C1−C3 and C500−C502: The component τ_3 shows little change but the corresponding intensity I_3 decreases. Concurrently, $I_{12} = 1 - I_3$ increases, but now the corresponding lifetime τ_{12} also increases and eventually reaches values up 0.130 to 0.136 ns.

Supplemental Fig. 1 shows τ_{1C} measured at 20 °C with spectrometer *B* for state C1500 during long natural ageing at 'room temperature'. Merely fluctuations on the scale of ≤ 1 ps are found.

Fig. 7 shows results of the CDB measurements. Fig. 7a displays measurements at 'room temperature' for well annealed pure Ni and Ti as well as for samples in the states AN, C1 and C500. All NiTi curves lie between the curves obtained for the pure elements. Cycling shifts the curves towards Ti. Fig. 7b shows one measurement each for C1 and C500 at 20 and −120 °C. The lower the temperature, the closer the measured response to the one of Ni.

5. Discussion

5.1. Possible positron trapping sites

In crystals completely free of defects, a positron is delocalized in the lattice and the electron density in inter-atomic regions determines its lifetime (so called bulk positron lifetime, τ_B). Higher electron density implies a shorter τ_B. For NiTi in the B2 structure, a τ_B value of 0.132 ns is reported [9], which is in a reasonable agreement with the bulk lifetime of the B2 structure obtained by our *ab-initio* calculations, see Table 1.

Single vacancies in an otherwise perfect crystal are efficient positron trapping sites due to their negative apparent charge at and below 'room temperature' since the depth of the associated potential well (a few eV) is much larger than the thermal energy of the positron (tens of meV). Provided that the site fraction of vacancies is larger than $\sim 10^{-7}$ sufficiently many positrons annihilate in them to give rise to a component showing in positron lifetime spectra. The lifetime of a positron trapped in such a deep trap is usually ~50% higher than in the bulk. The calculated lifetimes of positrons trapped in Ni (V_{Ni}) and Ti (V_{Ti}) vacancies are listed in Table 1. Relaxation of the nearest neighbour (NN) ions (i.e. Ti ions in the case of V_{Ni} and Ni ions in the case of V_{Ti}) and the next-nearest neighbour (NNN) ions (i.e. Ni ions for V_{Ni} and Ti ions for V_{Ti}) surrounding vacancies obtained by *ab-initio* calculations are listed in Table 1 as well. For V_{Ni} NN, Ti ions slightly relax from their regular lattice sites towards the vacancy while NNN Ni ions exhibit outward relaxation. The situation is reversed for V_{Ti} where relaxation of NNN Ni ions is outward while NNN Ti ions are displaced towards the vacancy.

From calculated positron biding energies E_B given in Table 1 one can deduce that V_{Ti} is a slightly deeper positron trap than V_{Ni} and is characterized by larger open volume, but the lifetimes of positrons trapped at V_{Ni} and V_{Ti} are similar. A

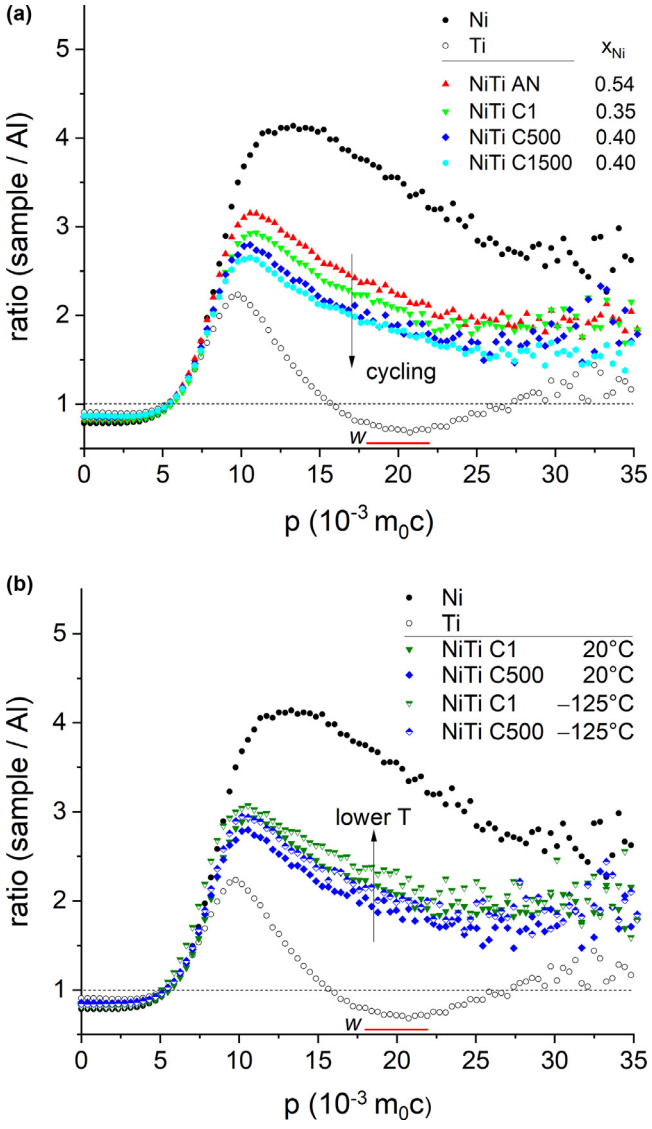

Fig. 7. (a) CDB measurements at 20 °C for states AN, C1, C500 and C1500 given as a ratio of the NiTi CDB data to that of annealed aluminium. 4 values for the Ni content of the environment of the annihilation site are given (bulk for AN, SV defects for Cn). Horizontal bar marks range in which w_i in Eqs. (4) and (8) were calculated to yield the values for x_{Ni} displayed here and discussed in the text. (b) Temperature-dependent Doppler broadening measurements for C1 and C500.

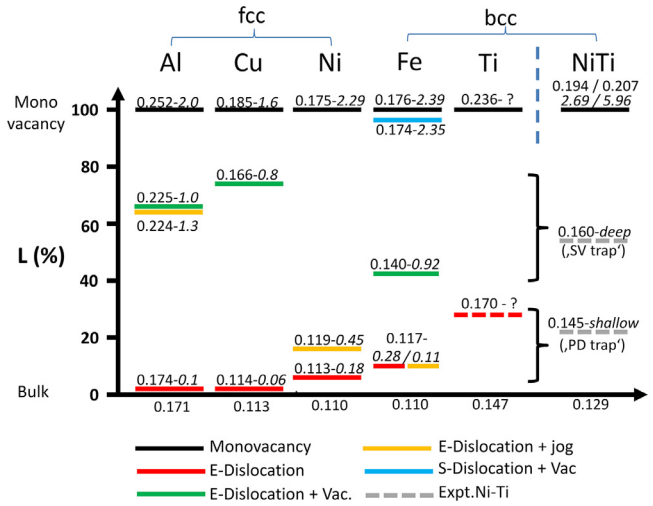

Fig. 8. Various calculated positron lifetimes τ_{disl} associated to edge (E) and screw (S) dislocation-related defects in Al, Cu [37], Fe [54], Ni [55], and Ti [56,57] shown as quantity L relative to the lifetimes in the bulk τ_B (bottom) and in a mono-vacancy τ_V (top), i.e. $L = (\tau_{disl} - \tau_B)/(\tau_V - \tau_B)$. The lifetime (in ns) is given together with the positron binding energy in eV (italics), Full lines: calculated, broken lines: measured. The figure provides an overview of positron lifetimes in different defects in various fcc and bcc metals and allows to assess the two lifetimes determined experimentally for Ni-Ti alloys (right column) relative to these elements. PD traps are found to be in the range usually occupied by dislocations or jogs (red lines, shallow traps), whereas SV traps are located in the range of dislocations in association with vacancies (green lines, deep traps). Dislocation jogs (orange lines) and screw dislocations (light blue) might also play a role. Thus, the identity claimed for the two traps in this paper is in accordance with that in pure elements. (For interpretation of the references to color in this figure legend, the reader is referred to the web version of this article.)

lifetime $\tau_V = 0.197$ ns of positrons trapped in vacancies generated by electron irradiation was reported for the B2 phase [9]. This experimental value corresponds well to the average of V_{Ni} and V_{Ti} in the B2 phase (0.201 ns).

Dislocations can also trap positrons but their potential well is of the same depth as the energy of the positron at 'room temperature'. Therefore, they are shallow positrons traps [36] and positrons can easily be de-trapped at 'room temperature'. Only at low temperatures, dislocations become deep enough to trap positrons long enough to give rise to a measurable lifetime component, i.e. they are 'activated' by lowering the temperature. However, dislocations can also act indirectly when positrons annihilate in open volume associated to them. Such open volume defects can be dislocation jogs or vacancies attached to dislocations [36,37]. While there is a general agreement that vacancies bound to dislocations act as deep positron traps, the role of jogs is disputed. Some researchers ascribe a significant role in annihilation to jogs [37,38], others find little open volume and see jogs acting similar to undisturbed edge dislocations [39]. Since a dislocation is a line defect with one macroscopic dimension while a vacancy is a point defect, the cross section for positron trapping in dislocations is much larger than that for vacancies. Hence, positron trapping in open volume defects associated with dislocations is a two-stage process: once a positron is weakly localized in the shallow potential of a dislocation line, it quickly diffuses along the dislocation line until it is finally trapped in a deep trap of the vacancy-like defect associated with the dislocation [40]. Fig. 8 gives (mostly) calculated positron lifetimes in various positron traps together with the binding energy between positron and traps for the 5 elements Al, Cu, Ni, Fe and Ti. All these lifetimes are normalised to the range between bulk lifetime (always lowest) and mono-vacancy lifetime (highest). On the very right the positron lifetimes in the two traps generated in NiTi are given as derived in this paper. It will be discussed in the following how they compare to the positron lifetimes given for the elements.

5.2. Annealed alloy (AN)

DSC data in Fig. 1 shows that during cooling there is a phase transition in two stages, first to the R phase than to the final martensitic B19' phase. The occurrence of the R phase stems from the slow cooling after solutionizing, as after quenching no such DSC peak is observed [15]. A possible explanation would be that during slow cooling, time is spent in the intermediate temperature range where Ti_3Ni_4 might precipitate. Annealed stoichiometric NiTi alloys have been found to show a direct transition to the B19' phase and the R phase appears only after a few (about 10) thermal cycles [41]. However, Ti_3Ni_4 was neither observed in the TEM images nor in the diffraction patterns. Precipitation during quenching has been observed by SANS, and the corresponding particles formed are just 2 nm in diameter [42], which explains their absence in TEM images. The low volume fraction of such parti-

cles would not alter the Ni concentration in the matrix enough to markedly modify M_s, but might be sufficient to induce *R* phase upon cooling.

The one-component positron lifetime τ_{1C} at 20 °C is 0.125 and 0.131 ns for two different samples measured with spectrometer *B*, see Fig. 4 (inset). The slight difference is due to different calibrations of the instrument. Spectrometer *P* yields an average positron lifetime $\bar{\tau} = 0.129$ ns when measured at 20 or 25 °C (Fig. 5). The literature value for B2 NiTi structure is 0.132 ns [9], thus fitting well to our measured values.

$\bar{\tau}$ shows a weak temperature dependence upon cooling. First, a slight increase from 0.129 to 0.131 ns, followed by a decrease to 0.127 ns (Fig. 5). This points at the martensitic transformation that changes the electron density due to a transformation from the B2 structure (NiTi austenite) to the intermediate *R* phase or the B19' structure (martensite). With our *ab-inito* calculations yielding the bulk positron lifetimes 0.127 ns for the B2 structure (NiTi), 0.131 ns for the R phase and 0.129 ns for the B19' phase (martensite) the observed changes are explained. The lifetime decrease in the second temperature step is partially also caused by the lattice contraction at lower temperature. The behavior of τ_{1C} measured at various temperatures with spectrometer *B* is similar to that of $\bar{\tau}$: τ_{1C} first increases to 0.135 ns upon cooling to −120 °C, after which it decreases to 0.129 ns at −180 °C (data not shown).

Literature data on various Ni-Ti alloys also show a pronounced lifetime increase with decreasing temperature, but the samples used there were annealed at 1000 °C and then quenched [12]. Positron lifetime was measured from 52 to −53 °C. A pronounced increase of positron lifetime (just one component reported in that study) is measured from ∼0.126 ns at 20 °C to ∼0.148 ns for a Ni content of 51%. The maximum occurs at the M_s temperature of −53 °C, i.e., the main increase is pre-martensitic. For 50.5% Ni, an M_s of 20 °C and a positron lifetime of 0.152 ns are found. Our sample (50.55 at.% Ni) in the 'AN' state, however, does not reach values higher than 0.135 ns at any temperature and the highest value is found far below M_f (not shown in Figures). The only feature reported in Ref. [12] we can confirm is the decrease towards lower temperatures, however with a smaller amplitude.

Fig. 6b shows that there is only one lifetime component in the 'AN' sample at 25 °C and also at lower temperatures. Together with the small temperature dependence this points at predominant positron annihilation in the bulk of the austenite or martensite structure. Dislocations or other defects do not play a role since they are shallow and would give rise to a temperature dependence of the positron lifetime and to more than one lifetime component at low temperature. This finding is actually in variance with results reported on similar alloys first melt-spun, and then annealed at 1000 °C and furnace cooled, in which still 70% or 78% of the annihilation was in traps with typical lifetimes of 0.161 or 0.171 ns, respectively [8]. The same applies to another reported measurement [43], where in the annealed state $\bar{\tau}$ values above 0.160 ns were measured. The temperature dependence of $\bar{\tau}$, in turn, was similar to what is reported here, just shifted to much higher values by about 0.04 ns [43]. Perhaps some (undocumented) thermal cycling was carried out in those studies or additional defects were included during manufacture. We think that our result is the correct one because a lower defect density is more difficult to achieve and the data were measured independently with two spectrometers.

The CDB ratio curve of the state AN lies between that of pure Ni and Ti (roughly in the middle, Fig. 7a). This can be expected due to a near equal content of Ni and Ti in the ordered B2 lattice in which the positrons annihilate. As chemical information about the neighbourhood of the annihilation site is provided by the high momentum data due to the interaction of positrons with the core electrons of the surrounding atoms, we determine an average value w_i for each curve *i* in Fig. 7a in the momentum range indicated by the horizontal bar. By writing

$$w_{\mathrm{NiTi,\ AN}} = x_{\mathrm{Ni}} w_{\mathrm{Ni}} + (1 - x_{\mathrm{Ni}}) w_{\mathrm{Ti}}, \tag{4}$$

we obtain a fraction x_{Ni}= 0.54 of Ni atoms in the neighbourhood of the (average) annihilation site (delocalised in the bulk) which close to the nominal site fraction of 0.505 Ni.

Altogether, the annealed state is consistently described by all the measurements as a state with a low level of defects that do not contribute to positron annihilation at any of the investigated temperatures. We shall use the value $\tau_B = 0.129$ ns for the lifetime of a positron in the undisturbed NiTi lattice in the following discussion.

5.3. Cycled state C1

The measurements at 'room temperature' show that compared to the annealed state AN, in state C1 both τ_{1C} (Fig. 4, spectrometer *B*) and $\bar{\tau}$ (Fig. 5, spectrometer *P*) are increased by about 3 ps. This points at the formation of defects associated with additional open volume. Such defects trap positrons and increase the measured average positron lifetime.

The TEM images show a pronounced increase in image contrast after one cycle, namely the appearance of a high number density of particles causing 'coffee-bean' contrast. Such contrast is typical for coherent strain fields around precipitates or particles. Both electron and X-ray diffraction studies show that the particles are predominantly *R* phase, which is metastable at 'room temperature' and should have dissolved during reheating but has been possibly stabilised by the effects of mechanical straining during thermal cycling. Such residual *R* phase has not been reported in other cycling studies. However, those usually include an upper temperature of the thermal cycle higher than in the current study (100 °C: [4,5], 150 °C [44], 67 °C only for equiatomic NiTi [41]) so that residual *R* phase might have dissolved there. The presence of such a dense distribution of phases is linked to the absence of a network of dislocations well visible in the homogenous austenitic lattice as reported by Pelton et al. [5]. Rather, we hypothesize the presence of a high density of misfit dislocations hidden in the strain contrast around the residual phases but giving rise to a temperature-dependent positron lifetime signature, see Sec. 5.4 on the C500 sample.

Another characteristic of thermal cycling is that M_s is shifted by just about 3 K. The same applies to the reverse transformation. This is in contrast to reports on strong DSC peak shifts of the forward and reverse transformations [4,5,41,44]. The observed value for M_S of −32 °C in Fig. 1 is much lower than the M_S of 2.1 °C reported for the AQ state [15]. This observation suggests that the full effect of hindering the transformation to martensite has unfolded already in the first cycle.

Fig. 6a, b yield more information. Two positron lifetime components are measured at 20 °C with the spectrometer *P* defining a mixture of 69% of $\tau_{12} = 0.118$ ns and 31% of $\tau_3 = 0.160$ ns. Here we call the second component τ_3, anticipating that the component τ_{12} will be split into two components later (at low temperatures). At 'room temperature' τ_{12} could be simply written as τ_1 since the intensity of τ_2 is near zero, but this would complicate notations. Using the equation of the two-state trapping model (2STM) that allows one to calculate the bulk lifetime τ_B [45]:

$$\tau_B^{\mathrm{calc}} = \left(\frac{I_{12}}{\tau_{12}} + \frac{I_3}{\tau_3} \right)^{-1}, \tag{5}$$

yields the value of 0.128 ns given in Fig. 9a (discussed in Section 5.6). This shows that the 2STM is fulfilled reasonably well since τ_B^{calc} is close to the value for the annealed state (0.129 ns) that represents annihilation in the bulk of the B2 structure.

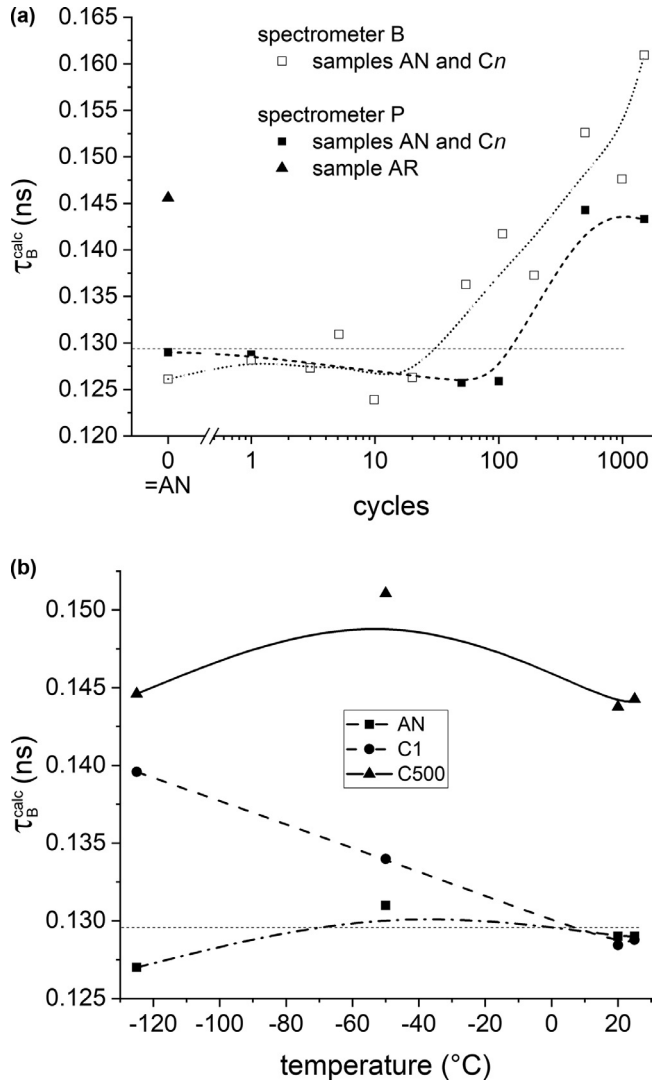

Fig. 9. τ_B^{calc} calculated with Eq. (5) based on two-state trapping model (2STM) for various measurements reported in this paper. (a) 'room temperature' measurements for different cycle numbers and for the as-received material, (b) measurements at spectrometer *P* for 3 different temperatures and 3 different states.

The positron lifetime $\tau_3 = 0.160$ ns represents a new trap created by thermal cycling. Potential candidates are deep vacancy-related objects such as a bare vacancy, a vacancy-solute complex or a dislocation with an attached vacancy. Bare vacancies in NiTi are expected to have τ values of 0.197 ns as found for irradiated NiTi [9] and therefore cannot be the source of τ_3. A better candidate is a vacancy that is attached to a dislocation and is therefore squeezed in volume by the compressive stress field of the dislocation. As the formation energy of vacancies at a dislocation can be markedly lower than in the bulk [37] it is plausible that cycling induces such squeezed vacancies ('SV') that then remain associated to dislocations. We shall call this object '*SV trap*' in the following. The positron lifetime in this trap is about 50% on the normalised scale between τ_B and τ_V, which is about the same as for various elements, see green lines in Fig. 8. The other component ($\tau_{12} = 0.118$ ns) is the reduced lifetime of free positrons. It is only slightly reduced to below the value for bulk annihilation because $I_{12} = 69\%$ is so high.

The temperature dependence of the positron lifetime decompositions during cooling to −50 and −125 °C yields additional information. In Fig. 6b, τ_{12} increases from ∼0.118 to ∼0.135 ns, I_{12} increases by ∼10%, while τ_3 remains the same but I_3 decreases by ∼10% upon cooling to −125 °C. This temperature dependence implies that a shallow trap is 'activated' at low temperatures, i.e. due to a lower measurement temperature the positrons can now annihilate in the trap and contribute to the signal. A good candidate for such a trap is a 'pure' dislocation ('PD'), i.e. without an attached vacancy. It will be called '*PD trap*' in the following.

The positron lifetime in a dislocation line is usually (at least for elemental Al, Cu, Ni, Fe) very close to the bulk lifetime and binding of a positron is weak (red lines in Fig. 8). So shallow traps characterized by a lifetime slightly higher than that of the bulk explain the experimental findings. Whether jogs on edge dislocations fall into the category of shallow traps is disputed (compare Al and Ni/Fe in Fig. 8 given by orange lines). If yes, jogs could be the annihilation sites. Moreover, there is a chemical preference for Ni in the environment of the annihilation sites since CDB indicates an increase in the contribution of positrons annihilating with core electrons of Ni at low temperatures (Fig. 7b). We will discuss in the next section why the *R* phase itself is not considered the source of positron trapping.

As positrons can annihilate in two different traps and in the bulk, the 3-state trapping model (3STM) should be applied implying that there are three measurable lifetime components, τ_1, τ_2 and τ_3. However, due to limited spectrometer resolution, only two lifetimes are actually resolved, namely τ_{12} and τ_3.

The positron lifetime τ_2 in the 'activated' shallow (PD) trap cannot be larger than 0.160 ns because in this case the spectrometer would have mixed the contribution of the deep trap (dislocation with a squeezed vacancy) with the shallow trap (dislocation) and a higher value and intensity of τ_3 would have been the consequence. On the other hand, τ_2 cannot be smaller than τ_{12} since $\tau_1 < \tau_2$ and $I_{12}\tau_{12} = I_1\tau_1 + I_2\tau_2$ with $0 \le (I_1, I_2) \le 1$. Thus, 0.129 ns $= \tau_1 \le \tau_{12} \le \tau_2 \le \tau_3 =$ 0.160 ns.

We rationalise this by stating that: (i) The value $\tau_{12} = 0.135$ ns measured at −125 °C (Fig. 6b) is in reality a mixture of a reduced free positron contribution (τ_1) and the lifetime of positrons confined in the shallow PD trap (τ_2). (ii) As mentioned above, τ_2 must be between τ_{12} and 0.160 ns. The largest τ_{12} measured is 0.135 ns. We estimate that τ_2=0.145 ns, which is roughly in the middle between the lifetime in the SV trap (∼0.160 ns) and in the bulk lifetime (∼0.129 ns). This choice appears reasonable because the positron lifetime in an undisturbed dislocation should be close to the lifetime in the bulk τ_B=0.129 ns. Therefore, we chose a value close to the lower limit of 0.135 ns. (iii) The 3STM is satisfied. (iv) At −125 °C, the shallow PD trap is nearly fully 'activated'. The 3STM defines $\bar{\tau}$ in term of three lifetimes and two independent intensities:

$$\bar{\tau} = I_1\tau_1 + I_2\tau_2 + I_3\tau_3; I_1 + I_2 + I_3 = 1 \quad (6)$$

Here, the left hand side is a known measured quantity, but as $I_1$and $\tau_1$are unknown, the equation is underdetermined. However, due to assumption (iii) we can write [45]:

$$\tau_B = \left(\frac{I_1}{\tau_1} + \frac{I_2}{\tau_2} + \frac{I_3}{\tau_3}\right)^{-1} = 0.129\text{ns}, \quad (7)$$

which allows us to determine $I_1$and τ_1 (and hence $I_2 = 1 - I_1 - I_3$) by combining Eqs. (6) and (7) and solving a second order equation. The result is I_1=9%, τ_1 =0.055 ns and I_2=70%, τ_2 = 0.145 ns, see Fig. 10a that also shows values for −50 °C. For the 'room temperature' measurement $I_2 \sim 0$ is required since the 2STM is satisfied for τ_{12} and τ_3. Fig. 10a shows that starting from 'room temperature', where we find a low contribution of PD traps, for decreasing temperature PD traps gain importance in absolute terms (increasing I_2 at the cost of mainly the free positron contribution I_1) but also relative to the SV traps since I_3 decreases. At −125 °C, the effect of PD traps is 3.3 times higher than that of SV traps.

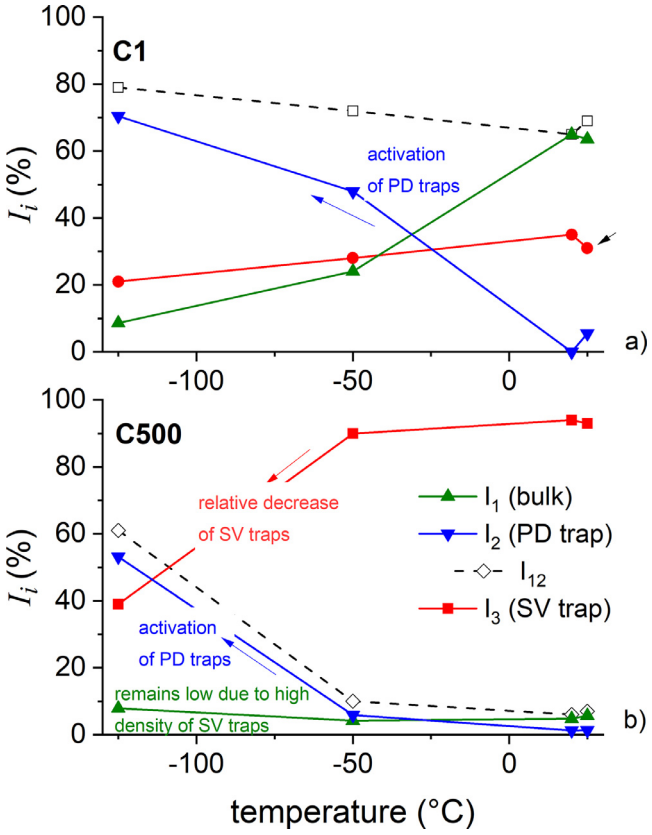

Fig. 10. Decomposition of positron lifetime component τ_{12} into τ_1 and τ_2 in (a) C1, (b) C500 sample based on the 3STM. $\tau_2 = 0.145$ ps was used and only intensities are shown. τ_3 is almost constant (~0.160 to ~0.171 ns, see Fig. 6 (b) so that only τ_1 exhibits considerable variation. The values for τ_{12} and I_{12} can be read from Fig. 6b.

The CDB ratio curve is shifted towards Ti by cycling compared to the annealed state (Fig. 7a). The shift is caused by a decrease of the Ni fraction in the environment of the annihilation site. Using the averages w_i in the high-momentum regime defined in the last paragraph we can calculate the Ni site fraction $x_{\mathrm{Ni,C1}}$ using:

$$w_{\mathrm{NiTi,\ C1}} = (1 - I_3) w_{\mathrm{NiTi,\ AN}} + I_3 [x_{\mathrm{Ni,C1}} w_{\mathrm{Ni}} + (1 - x_{\mathrm{Ni,C1}}) w_{\mathrm{Ti}}]. \quad (8)$$

Here, $I_3 = 0.31$ is taken from Fig. 10a (see arrow) yielding $x_{\mathrm{Ni}} = 0.35$. Therefore, cycling introduces traps with a Ti-enriched environment of the annihilation site and $x_{\mathrm{Ni}} = 0.35$ instead of $x_{\mathrm{Ni}} = 0.54$ as in the AN state. Thus, the squeezed vacancy is preferentially a missing Ni atom surrounded by Ti or Ti has segregated to the annihilation site. This finding is in agreement with calculations in which the equilibrium site fraction of vacancies was calculated for B2 NiTi and vacancies on Ni sites were found to be much more numerous than vacancies on Ti sites (many orders of magnitude, although still a low fraction) [46]. Non-equilibrium vacancies created by thermal cycling would then show the same preference for Ni sites.

At −125 °C, the Doppler spectrum is closer to Ni than at 20 °C (Fig. 7b). The PD trap activated at low temperature shows more annihilation through Ni atoms. Therefore, either the entire dislocation line or the jogs have a slight preference for Ni in their immediate neighbourhood.

5.4. Cycled state C500

500 cycles have only a small effect on the DSC traces as the peaks of the cooling curve are shifted only slightly (3 K) to lower temperature (Fig. 1) unlike in cases where shifts are an order of magnitude larger [4]. However, this is not a contradiction since even shifts to higher temperature are known in some alloys [7]. In this particular case, the absence of dislocations after slow cooling as opposed to the usual quenching is one reason for the absence of the shift. Another is the occurrence of residual *R* phase after the first cycle. Together, these prevent the gradual build-up of a dislocation network and the associated shift of the peak positions as discussed in Ref. [5].

PALS measurements at 'room temperature' show that compared to state AN and C1, 500 thermal cycles markedly increase the positron lifetime measured at either 20 or 25 °C. For spectrometer *B*, τ_{1C} increases by 36–38 ps to 0.161–0.163 ns (Fig. 4), for spectrometer *P*, the increase for $\bar{\tau}$ is 32–37 ps to 0.161–0.166 ns (Fig. 5). This is much more than for state C1 and indicates further formation of SV traps. However, TEM images have a similar appearance after 1 or 500 cycles or more, see Fig. 2c–e. Whether high cycle numbers further increase the number of *R* phases is not clear from the TEM images. If yes, it is not a very pronounced increase, whereas positron lifetime does show large further changes. This leads to the conclusion that the particles visible so clearly cannot cause the increase of positron lifetime directly. Rather dislocations attached to the *R* phases trap positrons. As no dislocations are visible in the space between the *R* phases these must be very short and associated to the phases. There, very strong stress obscures these phases. Misfit dislocations can be created as the stress during continued growth of *R* during cycling is partially relaxed. They increase in number as the stresses in each cycle increase. The relationship between such misfit dislocations and the specific 'coffee-bean' contrast observed has been described in the literature [47].

The two-component decomposition in Fig. 6 measured at 20 °C by spectrometer *P* yields 7% of $\tau_{12} = 0.049$ ns and 93% of $\tau_3 = 0.169$ ns, showing that compared to state C1, the contribution related to SV traps is close to saturation and just a small free positron contribution is left. As Fig. 4 shows that the increase of τ_{1C} saturates after 500 cycles (or earlier) it is reasonable to assume that SV trap formation has come to an end in sample C500 or that saturation trapping is reached.

Due to the predominance of SV traps the reduced free positron lifetime $\tau_1 = 0.049$ ns at 20 °C is very small. In the 2STM, $I_1 \to 0$ as $\tau_1 \to 0$. This is in accordance with very small value $I_1 = 7\%$ observed.

As for C1, the temperature dependence of positron lifetime provides more information: Upon cooling to −125 °C from 'room temperature', τ_3 remains essentially unchanged but I_3 decreases sharply from 94 to 39%, see Figs. 6b and 10b. Correspondingly, τ_{12} increases from 0.049 ns to 0.132 ns, I_{12} by 55%. As for C1, the shallow PD trap is activated at low temperatures. Using the same typical positron lifetime in PD traps as for C1, $\tau_2 = 0.145$ ns and by applying Eqs. (5) and (6) again, τ_1 and I_1 can be determined. Fig. 10b shows the results that can be compared to the results for state C1 (Fig. 10a). For −125 °C we find $I_1 = 8\%$ and $\tau_1 = 0.045$ ns. The main differences between C1 and C500 are the following. In state C500, the intensity ratio I_2/I_3 is 1.4 while it is 3.3 in C1. Although the density of PD is higher in both cases, more SV traps have been created in state C500 than PD traps. In other words, with increasing number of cycles the concentration of SV traps increases faster than the concentration of PD traps. This is in accordance with a high concentrations of vacancies reported in materials subjected to severe plastic deformation [48,49].

The changes of $\bar{\tau}$ in Fig. 5 between low and high temperature are more pronounced than for state C1. This is due to the greater variability of I_3, i.e., higher concentration of SV traps, compare Fig. 10a, b. The Doppler spectrum at 20 °C is shifted even more towards Ti than for C1 and the temperature effect (shift towards Ni for lower *T*) is slightly stronger than for C1, see Fig. 7. Applying Eq. (8) using the data for C500 in Fig. 7a, we obtain a site fraction $x_{\mathrm{Ni}} = 0.4$ similar to that for state C1.

Table 2
Summary of the two types of positron traps formed during thermal cycling. Grey scale and number of large diamonds qualitatively indicate trap density.

object	short name	τ component	AN	C1	C500
Dislocations in a Ni-enriched environment	PD trap	τ_2	♦	◆◆	◆◆◆◆
Squeezed vacancies in a Ti-enriched environment associated to a dislocation	SV trap	τ_3	♦	◆	◆◆◆

♦ very small density, no clear positron signal.

5.5. Evolution from AN to C1 and C500

From the results obtained in Sections 5.2. to 5.4. one can conclude that one cycle applied to the annealed state introduces predominantly pure dislocations (shallow positron traps with a lifetime of 0.145 ns) and fewer squeezed vacancy/dislocation complexes (deep positron traps with lifetime 0.160–0.170 ns) as the free positron component at 'room temperature' is still large. Assuming that at −125 °C the shallow traps are fully activated, the intensity ratio between the latter and the former is 70:21. 500 cycles introduce more traps of both types than one cycle as reflected by a small bulk component at room temperature. The number of vacancy/dislocation complexes is relatively larger than after one cycle but pure dislocations still dominate (ratio 53:39). These facts are illustrated in Table 2.

5.6. Further aspects of measurements

The two-component decompositions in Fig. 6 allow us to estimate the defect density provided that a value for the specific trapping rate is known. For dislocations in Ni a value of $\mu = 2.9 \times 10^{15}$ s^{-1} has been reported [50] and we shall use this value for the NiTi alloy of the present study. It can be converted to an area-specific trapping rate of 2.3×10^{-4} m^{-2}s^{-1} (which is close to another value of 3.9×10^{-4} m^{-2}s^{-1} given in Ref. [51]). From this and the values for τ_{12}, τ_3 and I_3 we calculate the dislocation density associated to SV traps (PD dislocations not activated at 20 °C) using the 2STM,

$$\rho_D = \frac{I_3}{\mu}\left(\frac{1}{\tau_{12}} - \frac{1}{\tau_3}\right), \tag{9}$$

given in Fig. 11 as a function of the number of thermal cycles. The dislocation density strongly increases with increasing number of cycles from $\sim 10^{12}$ m^{-2} (typical for moderate deformations) and saturates in samples subjected to more than 500 cycles at a value around 7×10^{13} m^{-2} which corresponds to a heavily deformed metal. Note that Pelton et al., although applying different conditions, measure a comparable dislocation density range by TEM, namely from initially 10^{12} to 5×10^{14} m^{-2} at the end point of cycling including, however, all types of dislocations [5].

The deviations from the 2STM of all the positron lifetime data that can be decomposed into two components is expressed in Fig. 9 as the value τ_B^{calc} obtained from Eq. (5) and should be identical to the bulk lifetime $\tau_B = 0.129$ ns provided the 2STM is satisfied. The measurements approximately fulfilling the 2STM ($\tau_B^{calc} \leq 0.132$ ns) are states AN and the cycled states at 20 °C up to C100 for spectrometer *P*, up to C20 for spectrometer *B*. The 2STM is not fulfilled ($\tau_B^{calc} \geq 0.145$ ns) for the as-received sample AR, the higher cyled samples at 'room temperature' and also C1 and C500 at −125 °C. C1 at −50 °C and C50 to C200 at 20 °C (spectrometer *B*) show small deviations from the 2STM.

The trend that with increasing cycling (and hence creation of dislocations of both types) the 2STM is no longer fulfilled can be explained by taking into account that the annihilation centres are no longer uniformly distributed but lump together in certain spatial areas. Such an effect has been observed in ultra-fine grained Cu [52] and steel [53] prepared by severe plastic deformation. This supports the idea that dislocations are increasingly non-uniformly distributed after repetition of thermal cycling for many times and therefore cause the too high values of τ_B^{calc}. For C1, however, decreasing the temperature leads to the breakdown of the 2STM. This cannot be caused by non-uniform distribution of annihilation centres because after reheating to 'room temperature' the emerging state C2 satisfies the 2STM again. Here, a second reason is responsible, the presence of 3 positron lifetimes and the attempt to fit this with the 2STM instead of the 3STM. The middle component τ_2 might distribute over both measured components and lead to a wrong value of τ_B^{calc} as the equations of the trapping model show.

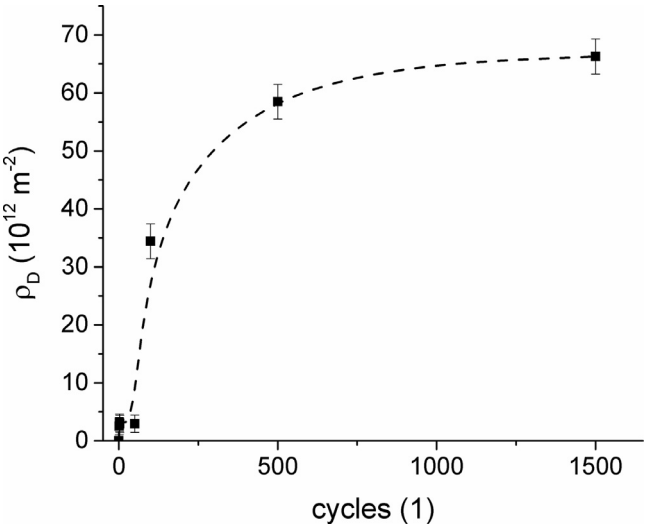

Fig. 11. The development of the mean density of SV traps with increasing number of cycles as calculated from PAS data using Eq. (9).

We also characterized the as-received (AR) materials before initial heat treatment. It is influenced by the manufacturing process involving rolling. We find two components, 46% of 0.183 ns lifetime and 54% of 0.124 ns. The average lifetime $\bar{\tau}$ is therefore close to that of C100, and the calculated value $\tau_B^{calc} = 0.146$ ns indicates that the 2STM is not satisfied. Therefore, AR can be assumed to contain non-uniformly distributed defects that were created during rolling.

6. Conclusion

Thermal cycling of a NiTi shape memory alloy (50.55 at% Ni) through the B2 ↔ (R) ↔ B19' martensite transition was studied by positron annihilation lifetime and coincidence Doppler broadening

spectroscopies and thermo-calorimetry. The main findings are supported by TEM and XRD measurements:

- The annealed and slowly cooled alloy is low in defects.
- In the first cycle, a high number density of 10 to 20 nm large particles of residual *R* phase but no Ni_4Ti_3 phases are formed. Positron trapping is initiated in misfit dislocations around these phases.
- Up to 300 to 500 cycles, more positron traps are generated in each cycle, after which defect generation saturates.
- Two types of positron traps can be distinguished, namely:
  - 'Pure' dislocation (PD). The annihilation site, possibly a jog, has a slightly Ni-enriched neighborhood.
  - Squeezed vacancy (SV): a vacancy is attached to a dislocation line and is squeezed in volume compared to a free vacancy. It is preferentially a vacancy on a Ni site.
  - Both dislocation types are concentrated near *R* phases.
  - No free monovacancies are found, i.e., their site fraction is $< 10^{-7}$.
- PD traps are formed earlier than SV traps and, when activated, their contribution to positron annihilation is always higher, but thermal cycling creates relatively more SV traps.

We have demonstrated that PAS is a suitable tool to detect subtle changes of defect configuration even after just one thermal cycle. It would be promising to extend the study to other shape memory alloys and other thermomechanical treatments.

Declaration of Competing Interest

The authors declare that they have no known competing financial interests or personal relationships that could have appeared to influence the work reported in this paper.

Acknowledgments

We acknowledge Christiane Förster and Claudia Leistner for their sample preparation, Leonardo Agudo Jácome for their help with TEM experiments, and Jürgen Olbricht and Philippe Vermaut for fruitful discussions. Computational resources were supplied by the project "e-Infrastruktura CZ" (e-INFRA LM2018140) provided within the program Projects of Large Research, Development and Innovations Infrastructures.

Supplementary materials

Supplementary material associated with this article can be found, in the online version, at doi:10.1016/j.actamat.2021.117298.

References

[1] G.L. Fan, K. Otsuka, X.B. Ren, F.X. Yin, Twofold role of dislocations in the relaxation behavior of Ti-Ni martensite, Acta Mater. 56 (2008) 632–641.
[2] K. Otsuka, X. Ren, Physical metallurgy of Ti-Ni-based shape memory alloys, Prog. Mater. Sci. 50 (2005) 511–678.
[3] S.K. Giri, M. Krishnan, U. Ramamurty, Enhancement of fatigue life of Ni-Ti-Fe shape memory alloys by thermal cycling, Mater. Sci. Eng. A 528 (2010) 363–370.
[4] S. Miyazaki, Y. Igo, K. Otsuka, Effect of thermal cycling on the transformation temperatures of Ti-Ni alloys, Acta Metall. 34 (1986) 2045–2051.
[5] A.R. Pelton, G.H. Huang, P. Moine, R. Sinclair, Effects of thermal cycling on microstructure and properties in Nitinol, Mater. Sci. Eng. A 532 (2012) 130–138.
[6] C. Grossmann, J. Frenzel, V. Sampath, T. Depka, G. Eggeler, Elementary transformation and deformation processes and the cyclic stability of NiTi and NiTiCu shape memory spring actuators, Metall. Mater. Trans. A Phys. Metal. Mater. Sci. 40A (2009) 2530–2544.
[7] T. Simon, A. Kröger, C. Somsen, A. Dlouhy, G. Eggeler, On the multiplication of dislocations during martensitic transformations in NiTi shape memory alloys, Acta Mater. 58 (2010) 1850–1860.
[8] P. Donner, R. Würschum, E. Hornbogen, H.E. Schäfer, Vacancy studies in melt-spun shape memory alloys by positron lifetime measurements, Scr. Metal. Mater. 25 (1991) 1875 1578.
[9] R. Würschum, K. Badura-Gergen, E.A. Kümmerle, C. Grupp, H.E. Schaefer, Characterization of radiation-induced lattice vacancies in intermetallic compounds by means of positron-lifetime studies, Phys. Rev. B 54 (1996) 849–856.
[10] H. Araki, N. Matake, P. Chalermkarnnon, Y. Shirai, Pre-martensitic phenomenon in NiTi studied by positron lifetime spectroscopy, Mater. Sci. Forum 327-328 (2000) 437–440, doi:10.4028/www.scientific.net/MSF.327-328.437.
[11] J. Katsuyama, P. Chalermkarnnon, M. Mizuno, H. Araki, Y. Shirai, Study of pre–martensitic phenomena in NiTi alloys by positron annihilation lifetime spectroscopy, Shape Mem. Mater. Appl. 394-3 (2002) 217–220.
[12] J. Katsuyama, T. Kobayashi, P. Chalermkarnnon, M. Mizuno, H. Araki, Y. Shirai, Anomalous temperature changes of positron lifetime and electrical resistivity in B2-NiTi alloys, Mater. Trans. 43 (2002) 1489–1493.
[13] J. Banhart, M.D.H. Lay, C.S.T. Chang, A.J. Hill, Kinetics of natural aging in Al-Mg-Si alloys studied by positron annihilation lifetime spectroscopy, Phys. Rev. B 83 (2011) 014101 (1–13).
[14] D.Q. Xue, Y.M. Zhou, X.B. Ren, The effect of aging on the B2-R transformation behaviors in Ti-51at%Ni alloy, Intermetallics 19 (2011) 1752–1758.
[15] V.V. Shastry, U. Ramamurty, Simultaneous measurement of mechanical and electrical contact resistances during nanoindentation of NiTi shape memory alloys, Acta Mater. 61 (2013) 5119–5129.
[16] J. Frenzel, E.P. George, A. Dlouhy, C. Somsen, M.F.-X. Wagner, G. Eggeler, Influence of Ni on martensitic phase transformations in NiTi shape memory alloys, Acta Mater. 58 (2010) 3444–3458.
[17] J. Banhart, M. Liu, Y. Yong, Z. Liang, C.S.T. Chang, M. Elsayed, M.D.H. Lay, Study of ageing in Al-Mg-Si alloys by positron annihilation spectroscopy, Phys. B Condens. Matter 407 (2012) 2689–2696.
[18] J. Kansy, Microcomputer program for analysis of positron annihilation lifetime spectra, Nucl. Instrum. Methods Phys. Res. Sect. A Accel. Spectrom. Detect. Assoc. Equip. 374 (1996) 235–244.
[19] F. Becvar, J. Cizek, I. Prochazka, J. Janotova, The asset of ultra-fast digitizers for positron-lifetime spectroscopy, Nucl. Instrum. Methods Phys. Res. Sect. A Accel. Spectrom. Detect. Assoc. Equip. 539 (2005) 372–385.
[20] H. Surbeck, Measurements of positron lifetime in AgBr crys tals, Helv. Phys. Acta 50 (1977) 705–721.
[21] J. Cizek, M. Vlcek, I. Prochazka, Digital spectrometer for coincidence measurement of Doppler broadening of positron annihilation radiation, Nucl. Instrum. Methods Phys. Res. Sect. A Accel. Spectrom. Detect. Assoc. Equip. 623 (2010) 982–994.
[22] R.S. Brusa, W. Deng, G.P. Karwasz, A. Zecca, Doppler-broadening measurements of positron annihilation with high-momentum electrons in pure elements, Nucl. Instrum. Methods Phys. Res. Sect. B Beam Interact. Mater. Atoms 194 (2002) 519–531.
[23] P. Sittner, P. Lukas, D. Neov, V. Novak, D.M. Toebbens, *In situ* neutron diffraction studies of martensitic transformations in NiTi, J. Phys. IV 112 (2003) 709–712.
[24] J. Khalil-Allafi, W.W. Schmahl, D.M. Toebbens, Space group and crystal structure of the *R*-phase in binary NiTi shape memory alloys, Acta Mater. 54 (2006) 3171–3175.
[25] S.D. Prokoshkin, A.V. Korotitskiy, V. Brailovski, S. Turenne, I.Y. Khmelevskaya, I.B. Trubitsyna, On the lattice parameters of phases in binary Ti-Ni shape memory alloys, Acta Mater. 52 (2004) 4479–4492.
[26] J.P. Perdew, A. Zunger, Self-interaction correction to density-functional approximations for many-electron systems, Phys. Rev. B 23 (1981) 5048.
[27] G. Kresse, J. Furthmüller, Efficient iterative schemes for ab initio total-energy calculations using a plane-wave basis set, Phys. Rev. B 54 (1996) 11169–11186.
[28] G. Kresse, J. Hafner, *Ab initio* molecular dynamics for liquid metals, Phys. Rev. B 47 (1993) 558.
[29] J.P. Perdew, in P. Ziesche and H. Eschrig (Eds.). Electronic Structure of Solids '91, Ed. P. Ziesche and H. Eschrig (Akademie Verlag, Berlin, 1991) 11.
[30] H.J. Monkhorst, J.D. Pack, Special points for Brillouin zone integrations, Phys. Rev. B 13 (1976) 5188.
[31] M.J. Puska, R.M. Nieminen, Theory of positrons in solids and on solid-surfaces, Rev. Mod. Phys. 66 (1994) 841–897.
[32] B. Barbiellini, M.J. Puska, T. Korhonen, A. Harju, T. Torsti, R.M. Nieminen, Calculation of positron states and annihilation in solids: a density-gradient-correction scheme, Phys. Rev. B 53 (1996) 16201–16213.
[33] T. Korhonen, M.J. Puska, R.M. Nieminen, First-principles calculation of positron annihilation characteristics at metal vacancies, Phys. Rev. B 54 (1996) 15016–15024.
[34] J.P. Desclaux, Multiconfiguration relativistic Dirac-Fock program, Comput. Phys. Commun. 9 (1975) 31–45.
[35] M.J. Puska, R.M. Nieminen, Defect spectroscopy with positrons-a general calculational method, J. Phys. F Metal Phys. 13 (1983) 333–346.
[36] C. Hidalgo, S. Linderoth, N. Dediego, Positron-trapping mechanism at dislocations in Zn, Phys. Rev. B 36 (1987) 6740–6745.
[37] H. Häkkinen, S. Mäkinen, M. Manninen, Edge dislocations in Fcc metals - microscopic calculations of core structure and positron states in Al and Cu, Phys. Rev. B 41 (1990) 12441–12453.
[38] C. Hidalgo, G. Gonzalezdoncel, S. Linderoth, J. San Juan, Structure of dislocations in Al and Fe as studied by positron-annihilation spectroscopy, Phys. Rev. B 45 (1992) 7017–7021.
[39] Y. Kamimura, T. Tsutsumi, E. Kuramoto, Calculations of positron lifetimes in a jog and vacancies on an edge-dislocation line in Fe, Phys. Rev. B 52 (1995) 879–885.
[40] L.C. Smedskjaer, M. Manninen, M.J. Fluss, An alternative interpretation of positron-annihilation in dislocations, J. Phys. F Metal Phys. 10 (1980) 2237–2249.

[41] H. Matsumoto, Transformation behavior with thermal cycling in NiTi alloys, J. Alloys Compd. 350 (2003) 213–217.
[42] M. Kompatscher, B. Demé, G. Kostorz, C.H. Somsen, E.F. Wassermann, Small-angle neutron scattering of precipitates in Ni–Ti shape memory alloys, Acta Mater. 50 (2002) 1581.
[43] Y.F. Hu, W. Deng, W.B. Hao, L. Yue, L. Huang, Y.Y. Huang, L.Y. Xiong, Microdefects and electron densities in NiTi shape memory alloys studied by positron annihilation, Trans. Nonferr. Metals Soc. China 16 (2006) 1259–1262.
[44] N. Zotov, V. Marzynkevitsch, E.J. Mittemeijer, Evaluation of kinetic equations describing the martensite–austenite phase transformation in NiTi shape memory alloys, J. Alloys Compd. 616 (2014) 385–393.
[45] R. Krause-Rehberg, H.S. Leipner, Positron Annihilation in Semiconductors, Springer, 1999.
[46] J.M. Lu, Q.M. Hu, L. Wang, Y.J. Li, D.S. Xu, R. Yang, Point defects and their interaction in TiNi from first-principles calculations, Phys. Rev. B 46 (2007) 094108 (1–7).
[47] L.L. Song, S.J. Liu, X.D. Mao, A new method for fast statistical measurement of interfacial misfit strain around nano-scale semicoherent particles, RSC Adv. 7 (2017) 28506.
[48] J. Cizek, M. Janecek, O. Srba, R. Kuzel, Z. Barnovska, I. Prochazka, S. Dobatkin, Evolution of defects in copper deformed by high-pressure torsion, Acta Mater. 59 (2011) 2322–2329.
[49] B. Oberdorfer, D. Setman, E.M. Steyskal, A. Hohenwarter, W. Sprengel, M. Zehetbauer, R. Pippan, R. Würschum, Grain boundary excess volume and defect annealing of copper after high-pressure torsion, Acta Mater. 68 (2014) 189–195.
[50] G. Dlubek, O. Brümmer, E. Hensel, Positron annihilation investigation for an estimation of the dislocation density and vacancy concentration of plastically deformed polycrystalline Ni of different purity, Phys. Status Solidi A Appl. Res. 34 (1976) 737.
[51] R. Krause-Rehberg, V. Bondarenko, E. E.Thiele, R. Klemm, N. Schell, Determination of absolute defect concentrations for saturated positron trapping – deformed polycrystalline Ni as a case study, Nucl. Instrum. Methods A 240 (2006) 719–725.
[52] J. Cizek, I. Prochazka, M. Cieslar, R. Kuzel, J. Kuriplach, F. Chmelik, I. Stulikova, F. Becvar, O. Melikhova, R.K. Islamgaliev, Thermal stability of ultrafine grained copper, Phys. Rev. B 65 (2002) 094106.
[53] J. Cizek, M. Janecek, T. Krajnak, J. Straska, P. Hruska, J. Gubicza, H.S. Kim, Structural characterization of ultrafine-grained interstitial-free steel prepared by severe plastic deformation, Acta Mater. 105 (2016) 258–272.
[54] Y. Kamimura, T. Tsutsumi, E. Kuramoto, Influence of dislocations on positron lifetime in iron, J. Phys. Soc. Jpn. 66 (1997) 3090–3096.
[55] E. Kuramoto, T. Tsutsumi, K. Ueno, M. Ohmura, Y. Kamimura, Positron lifetime calculations on vacancy clusters and dislocations in Ni and Fe, Comput. Mater. Sci. 14 (1999) 28–35.
[56] P. Hruška, J. Čížek, F. Lukáč, J. Knapp, S. Mašková, J. Drahokoupil, O. Melikhova, I. Procházka, Hydrogen-induced defects in titanium, Defect Diffus. Forum 373 (2018) 122–125.
[57] B. Kolev, T. Troev, E. Popov, S. Peneva, Positron lifetime calculations of defects in titanium, Proceeding of the AIP Conference, 2075, 2019.